Enhanced accuracy of rainfall–runoff modeling with wavelet transform

Chien-ming Chou

ABSTRACT

Wavelet transform (WT) is typically used to decompose time series data for only one hydrological feature at a time. This study applied WT for simultaneous decomposition of rainfall and runoff time series data. For the calibration data, the decomposed rainfall and runoff time series calibrate the subsystem response function using the least squares (LS) method at each scale. For the validation data, the decomposed rainfall time series are convoluted with the estimated subsystem response function to obtain the estimated runoff at each scale. The estimated runoff at the original scale can be obtained by wavelet reconstruction. The efficacy of the proposed method is evaluated in two case studies of the Feng-Hua Bridge and Wu-Tu watershed. The analytic results confirm that the proposed wavelet-based method slightly outperforms the conventional method of using data only at the original scale. The results also show that the runoff hydrograph estimated by using the proposed method is smoother than that obtained using a single scale.

Key words | hydrological time series, rainfall–runoff relationship, subsystem response function, wavelet coefficients, wavelet transform

Chien-ming Chou
Department of Design for Sustainable Environment,
MingDao University,
369 Wen-Hua Road, Peetow,
Changhua 52345,
Chinese Taiwan
E-mail: *jamin@mdu.edu.tw*

INTRODUCTION

Because Taiwan is located in the major typhoon track in the western Pacific Ocean, typhoons are an influential weather phenomenon in Taiwan, where short and steep upstream channels characterize all watersheds. Associated heavy rainfall and flooding are one of the disasters that cause the greatest loss to property and life in the area. It is, therefore, essential to study the relationship of the rainfall and runoff processes, and to develop a flood forecasting system to provide protection and warning systems.

Flood forecasting is based on rainfall–runoff relationship modeling. Conventional rainfall–runoff schemes employ a one-dimensional system response function (e.g., the unit hydrograph) to approximate the dynamic behavior of a rainfall–runoff relationship. Developed by Sherman in 1932, the unit hydrograph (UH) plays a critical role in predicting the runoff hydrograph. Although widely available for analyzing and simulating the rainfall–runoff process, most methods and models involve using the original hydrological time series data alone. In practice, studying hydrological time series is difficult because they are controlled and influenced by complex factors (Zhang *et al.* 2011). From a time-frequency perspective, each hydrological time series includes several frequency components (Wang *et al.* 2005). Using the component at only one scale to model a hydrological system makes the internal mechanism difficult to understand (Wang *et al.* 2005). The application of wavelet-based multi-resolution analysis (MRA) (Mallat 1989) can provide tools for modeling a hydrological system at various scales.

Wavelet analysis is an increasingly important tool for image and signal processing (Rao & Bopardikar 1998). Wavelet analysis has also been used to investigate rainfall–runoff relationships. Nakken (1999) applied continuous wavelet transform (CWT) to identify the temporal variability of rainfall and runoff data and to determine the relationship between them. Labat *et al.* (2000) used wavelets to explain the non-stationarity of karstic watersheds. In addition, wavelets have been applied to the development of runoff prediction models (Labat *et al.* 2000). Wavelet analysis of

doi: 10.2166/hydro.2012.041

rainfall rates and runoffs and wavelet rainfall–runoff cross-analysis offer relevant information on the temporal variability of the rainfall–runoff relationship.

Lane (2007) proposed that wavelet-based analysis can interpret runoff time series and evaluate rainfall–runoff model results. He indicated that the benefits of localization and the qualitatively low sensitivity of wavelet power and phase to wavelet selection are sufficient for further exploration of wavelet-based approaches to rainfall–runoff model evaluation. Chou (2007) developed an efficient wavelet-based model of nonlinear rainfall–runoff processes, and applied it to forecast floods in a river basin. Inspired by the theory of wavelet transform (WT) and Kalman filters, based on the excellent capacity of the Volterra model, a time-varying nonlinear hydrologic model was presented to approximate arbitrary nonlinear rainfall–runoff processes. His validation results confirmed the accuracy of the method for estimating runoff for small watersheds in Taiwan.

Nourani *et al*. (2009) combined wavelet analysis with the artificial neural network (ANN) to model Ligvanchai watershed rainfall–runoff processes in Tabriz, Iran. Their modeling results showed that the use of multi-scale time series data for rainfall and runoff as the ANN input layer enabled accurate prediction of both short- and long-term runoff discharges. Chou (2011a) developed a novel framework for considering wavelet denoizing in linear perturbation models (LPMs) and in simple linear models (SLMs). Denoized rainfall and runoff time series data were applied to the SLM and used as the smooth seasonal mean employed by the LPM. Noise was used as the perturbation term in the LPM. The denoized runoff and estimated runoff noise were summed to estimate the overall runoff in the LPM. The analytical results demonstrated that wavelet denoizing enhances the precision of rainfall–runoff modeling of the LPM.

The novel concept in this study is that a redundant WT can be used for simultaneously decomposing effective rainfall and direct runoff time series. The decomposed rainfall and runoff time series can calibrate system and subsystem response functions using the least squares (LS) method at various scales. The validation results were also obtained using the calibrated system and subsystem response functions at various scales.

This study is organized as follows: First, the redundant WT is introduced. Second, this study proposes the method of using the LS to identify the system response function. The effectiveness of the presented method is then evaluated in two case studies in two small watersheds in Taiwan. Finally, the results are discussed, and conclusions are drawn.

REDUNDANT WAVELET TRANSFORM

The CWT of a continuous function outputs a continuum of scales. However, the input data are generally sampled discretely, and may be in the form of hydrological time series. The discrete wavelet transform (DWT) of a vector is the outcome of a linear transformation that yields a new vector with dimensions equal to those of the primeval vector. This transformation is also known as decomposition, and can be performed efficiently using Mallat's MRA algorithm (Mallat 1989).

However, the orthonormal DWT requires that the input data have a number of values with an integer power of two. The number of scales is naturally limited by $\log_2$ of the number of values in the input. This limitation is inappropriate for a hydrological time series, especially for the short duration of typhoon events that occur in Taiwan.

Holschneider (1995) introduced the '*à trous*' wavelet decomposition. The fundamental concept that underlies multi-scale analysis or MRA is the application of a WT to decompose signals into different scales or resolution levels. The signal, which is decomposed into coarse scale, is either called approximation signal or smooth trend. The signal, which is decomposed into fine scale, is called detailed signal. The WT can be a connection among signals at various scales. In contrast, the input data of the *à trous* WT can take any value, enabling the number of scales to be unlimited. Not only is the *à trous* WT parsimonious, but the filter outputs can also be interpreted meaningfully (Aussem & Murtagh 2001). The calculation of wavelets is performed in a cascaded scheme, and reconstruction formula is used.

The *à trous* algorithm is a redundant WT. The procedure for decomposing the discrete hydrological time series $s(k)$ is firstly to perform successive convolutions using a discrete low-pass filter c (Aussem & Murtagh 2001).

$$s_{i+1}(k) = \sum_{l=-\infty}^{\infty} c(l)\, s_i(k + 2^i l) \tag{1}$$

where s_i denotes the approximation signal at scale i. The finest scale is used to specify the original hydrological time series $x(k)$, *i.e.*, $s_0(k) = x(k)$. The increase in distances between the sampled points ($2^i l$) explains the application of '*à trous*' to this method (Aussem & Murtagh 2001). The B_3 spline, defined as (1/16, 1/4, 3/8, 1/4, 1/16), is generally used in a low-pass filter c (Lee *et al.* 1999; Aussem & Murtagh 2001) to fulfill the compact support condition (required for a WT) and be point-symmetric. Wavelet coefficients w_i are obtained from determining the differences among successive smoothed versions of the signal (Aussem & Murtagh 2001).

$$w_i(k) = s_{i-1}(k) - s_i(k) \tag{2}$$

Wavelet coefficients provide the 'detailed' signal, which in practice can capture small but meaningful characteristics in the data. Such a characterization will not lose any information only if the original data vector can be reconstructed from the wavelet components. Moreover, the 'residual' terms s_p, which represent the 'background' data, are added to the wavelet coefficients. The set $\Re = \{w_1, w_2, \ldots, w_p, s_p\}$ represents the WT of the data, such as wavelet coefficients, up to a scale of p.

Aussem & Murtagh (2001) presented the wavelet expansion of hydrological time series, in terms of the approximation signal and wavelet coefficients.

$$x(k) = s_p(k) + \sum_{i=1}^{p} w_i(k) \tag{3}$$

Other advantages of the *à trous* WT are as follows (Chibani & Houacine 2003). (I) The evolution of the wavelet decomposition can be followed from scale to scale. (II) The algorithm generates a single wavelet coefficient series at each level of the decomposition. (III) Wavelet coefficients are computed for each location, facilitating the detection of a dominant feature. (IV) The algorithm is implemented easily. Additionally, the recursive computation of this algorithm is effective and can be achieved using filter banks (Lee *et al.* 1999).

IDENTIFYING THE SYSTEM RESPONSE FUNCTION

The rainfall–runoff process in a river basin is regarded as a system with a single input–output relationship. The aim of the study of such systems is to model historic data and predict further runoff by determining the input–output relationship from observed input–output data. The system response function describes the relationship between the input and output, and varies with the characteristics of the system or according to the natural law. When linear models are used, the goal is to describe or approximate the system response function.

The hydrological mechanism at each scale is unknown. Although several nonlinear models, such as ANNs, can be used to model the input–output relationship at each scale, they cannot be used to explore the subsystem characteristics at each scale. The linear system and subsystem response functions can be identified from the calibrated data, and represent the average characteristics at each scale. They were adopted in this study to model the rainfall–runoff process at each scale.

The SLM (Wei & Wang 2005) is a simple and conventional method used to estimate the system response function from the rainfall–runoff data. In this study, the SLM is used to model the rainfall–runoff relationship at each scale.

Let $I(t)$ and $Q(t)$ represent the rainfall and runoff time series of the watershed, respectively, and let $H(t)$ represent the system response function. The rainfall–runoff process is assumed to be a linear, time-invariant, and single input–output system. The function of the SLM system can be represented by a linear convolution equation (Wei & Wang 2005):

$$Q(t) = \int_0^t H(\tau) I(t - \tau) \mathrm{d}\tau \tag{4}$$

where τ is an integral variable.

Equation (4) can be applied in discrete form (Wei & Wang 2005):

$$Q(k) = \sum_{i=1}^{L} H(i) I(k - i + 1) \tag{5}$$

where L is the memory length of the watershed, $I(k-i+1)$ is the average rainfall at time $k-i+1$, $Q(k)$ is the runoff at time k, and $H(i)$ is a system response function.

Equation (6) reveals data error or incomplete assumptions about linearity (Wei & Wang 2005):

$$Q(k) = \sum_{i=1}^{L} H(i)I(k-i+1) + e(k) \tag{6}$$

where $e(k)$ is the random error term.

Equation (6) can be expressed using matrix equations (Wei & Wang 2005):

$$\mathbf{Q}_{N\times 1} = \mathbf{I}_{N\times L}\mathbf{H}_{L\times 1} + \mathbf{E}_{N\times 1} \tag{7}$$

where N is the total length of the hydrological data, and L is the memory length of a system response function.

The system response function $\boldsymbol{H}$ can be identified using the LS method. The essential principle of LS is to minimize the sum of the squares of the differences between the observed and estimated values. Equation (8) defines the objective function (Wei & Wang 2005):

$$\begin{aligned} J(\mathbf{H}) = \sum_{i=1}^{N} e^2(i) &= \mathbf{E}^{\mathrm{T}}\mathbf{E} = (\mathbf{Q}-\mathbf{I}\mathbf{H})^{\mathrm{T}}(\mathbf{Q}-\mathbf{I}\mathbf{H}) \\ &= \mathbf{Q}^{\mathrm{T}}\mathbf{Q} - 2\mathbf{H}^{\mathrm{T}}\mathbf{I}^{\mathrm{T}}\mathbf{Q} + \mathbf{H}^{\mathrm{T}}\mathbf{I}^{\mathrm{T}}\mathbf{I}\mathbf{H} \end{aligned} \tag{8}$$

The system response function can be derived by minimizing the objective function, such as $\min\{J(\mathbf{H})\}$ (Wei & Wang 2005):

$$\hat{\mathbf{H}} = [\mathbf{I}^{\mathrm{T}}\mathbf{I}]^{-1}[\mathbf{I}^{\mathrm{T}}\mathbf{Q}] \tag{9}$$

APPLICATION AND ANALYSIS

Study basin

This study demonstrates the feasibility of applying the wavelet-based method to modeling the rainfall–runoff process with the selection of the Feng-Hua Bridge and Wu-Tu watershed in southern and northern Taiwan, respectively, as the study area. The areas of the upstream watersheds of Feng-Hua Bridge and Wu-Tu are 139.69 and 203.00 km^2, respectively, as shown in Figure 1. From 1991 to 2000, a total of 14 and 18 typhoon or storm events over Feng-Hua Bridge and Wu-Tu watershed, respectively, were collected for case studies. Half of these events calibrated the model, whereas the other half verified the performance of the proposed method. In Tables 1 and 2, detailed information of calibrated and validated typhoon or storm events are provided, respectively.

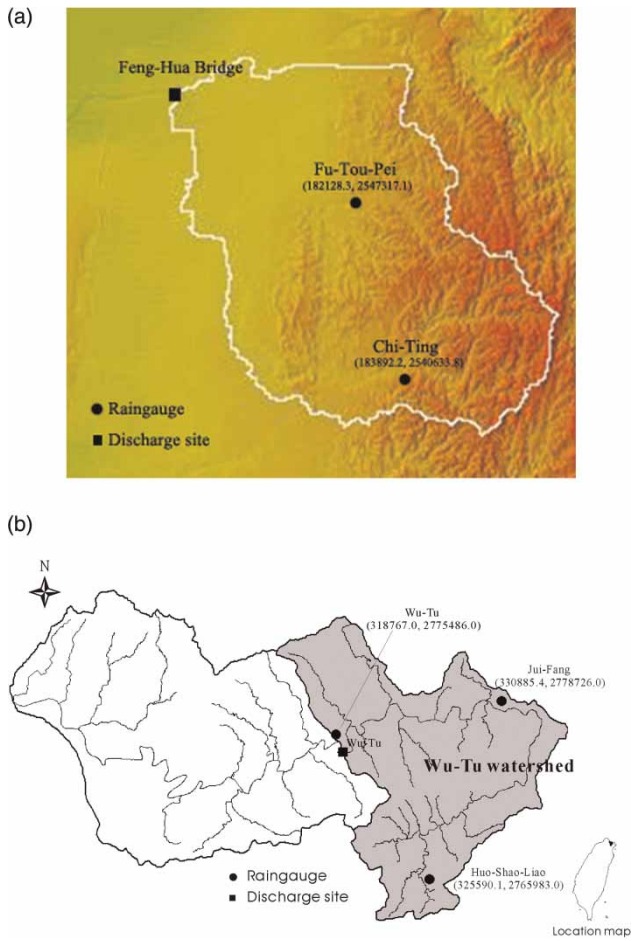

Figure 1 | (a) The topographical map of the upstream of the Feng-Hua Bridge watershed in the Yan-Shui River basin. (b) The map of the Wu-Tu watershed showing the study area near Taipei, Taiwan.

Table 1(a) | The detailed information of seven calibrated typhoon events for the Feng-Hua Bridge watershed

Events	Year	Duration (h)	Shape of peak	Peak discharge (m^3/s)
STORM (1991/07/28)	1991	96	Multiple	312.85
STORM (1992/07/04)	1992	144	Multiple	387.16
STORM (1992/08/30)	1992	48	Single	577.98
OMAR	1992	72	Single	416.89
TED	1992	48	Single	189.25
STORM (1993/06/11)	1993	48	Single	290.19
STORM (1993/08/13)	1993	48	Single	280.88

Table 1(b) | The detailed information of nine calibrated typhoon events for the Wu-Tu watershed

Events	Year	Duration (h)	Shape of peak	Peak discharge (m^3/s)
NAT	1991	40	Single	340
RUTH	1991	120	Multiple	583
POLLY	1992	84	Multiple	329
STORM (1994/06/18)	1994	42	Single	532
DOUG	1994	84	Multiple	344
FRED	1994	96	Single	252
GLADYS	1994	96	Single	439
SETH	1994	96	Multiple	481
HERB	1996	96	Single	1,090

Table 2(a) | The detailed information of seven validated typhoon events for the Feng-Hua Bridge watershed

Events	Year	Duration (h)	Shape of peak	Peak discharge (m^3/s)
TIM	1994	84	Single	339.97
CAITLIN	1994	72	Multiple	513.14
DOUG	1994	240	Multiple	356.66
HERB	1996	84	Single	264.37
STORM (1999/08/10)	1999	132	Multiple	243.24
STORM (2000/07/27)	2000	96	Multiple	363.60
BILIS	2000	84	Single	512.32

Table 2(b) | The detailed information of nine validated typhoon events for the Wu-Tu watershed

Events	Year	Duration (h)	Shape of peak	Peak discharge (m^3/s)
ZANE	1996	120	Multiple	678
WINNIE	1997	96	Single	1,040
STORM (1998/10/04)	1998	126	Multiple	428
ZEB	1998	102	Multiple	1,050
BABS	1998	198	Multiple	1,050
STORM (1999/12/13)	1999	222	Multiple	238
KAI-TAK	2000	120	Multiple	325
BEBINCA	2000	78	Multiple	632
STORM (2000/11/16)	2000	102	Multiple	191

Application

A redundant WT and SLM modeled the multi-resolution rainfall–runoff process. The first task is to simultaneously decompose the effective rainfall and the direct runoff time series by performing a redundant WT. Based on the decomposed rainfall and runoff time series data, the representative system and subsystem response functions are then estimated to model rainfall–runoff processes at various scales. Calibration to determine the system and subsystem response functions for a discrete linear model at various scales was performed using the decomposed rainfall and runoff time series data. In contrast, the validation procedure used the calibrated representative system and subsystem response functions in simulations to compare the fit to the observed data.

Comparison of model performances

In this study, LS and LS-WT represent the results of the adoption of the LS method without and with WT, respectively. To quantitatively compare the LS with LS-WT, the calibrated and validated results were evaluated based on five types of criteria. This work focuses on the fitness of

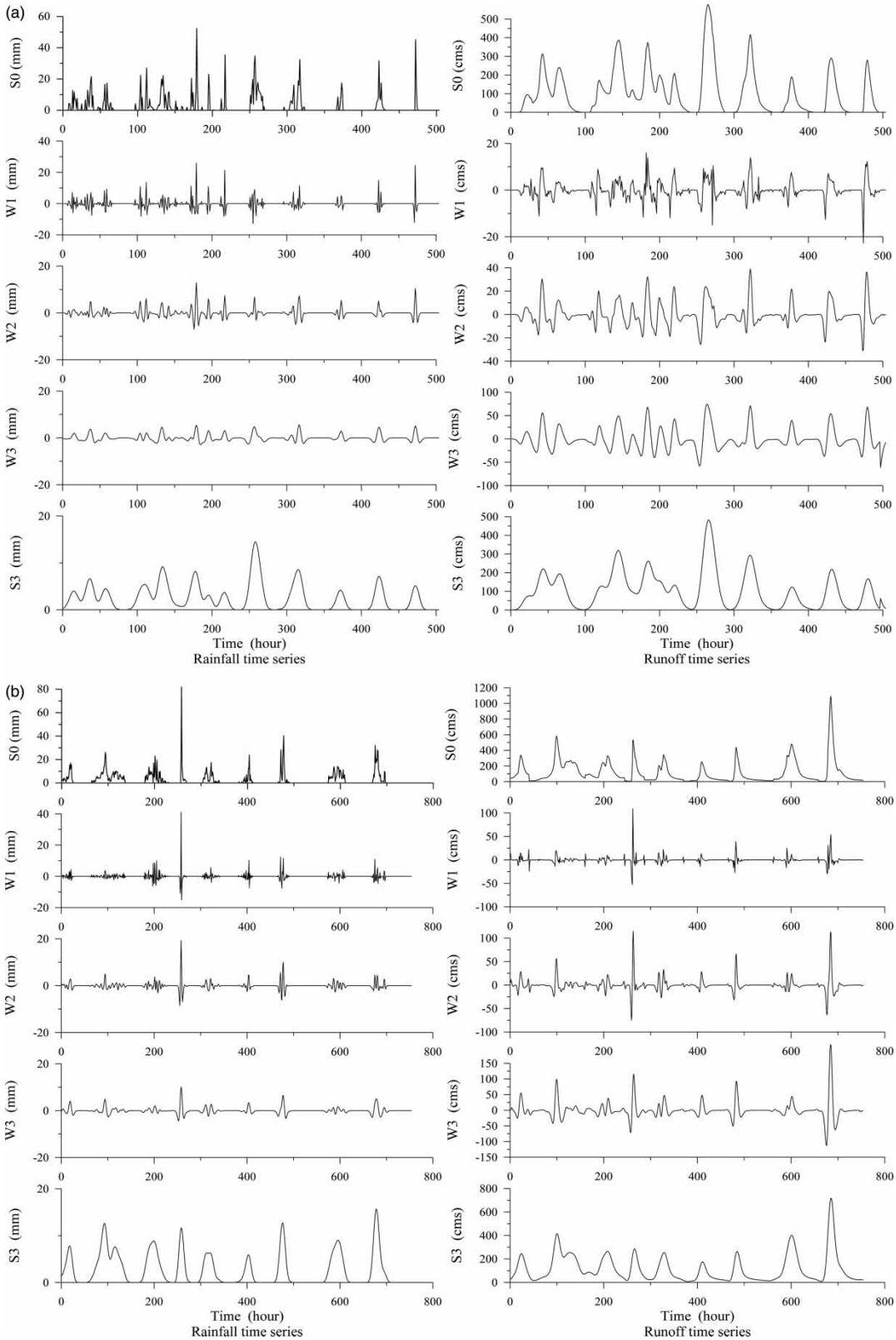

Figure 2 | Approximation (S3) and detailed signals (W1–W3) obtained using 3-level wavelet decomposition from the calibrated data. (a) Feng-Hua Bridge watershed. (b) Wu-Tu watershed.

Table 3 | The calibration results for all events in series using LS and LS-WT

Watershed	EV (%)		CE		COR		EQ_P (%)		ET_P (h)	
	LS	LS-WT	LS	LS-WT	LS	LS-WT	LS	LS-WT	LS	LS-WT
Feng-Hua Bridge	4.72	−0.87	0.897	0.922	0.949	0.960	1.90	−2.14	1	1
Wu-Tu	15.25	10.34	0.823	0.842	0.919	0.924	−35.93	−37.03	0	0

the estimated results as determined by the comparison with the observed data. The most important criterion is CE.

Coefficient of efficiency, CE

$$\mathrm{CE} = 1 - \frac{\sum_{i=1}^{N} [q(i) - \hat{q}(i)]^2}{\sum_{i=1}^{N} [q(i) - \bar{q}]^2} \tag{10}$$

where $\hat{q}(i)$ denotes the discharge of the simulated hydrograph for time i (m^3/s), $q(i)$ is the discharge of the observed hydrograph for time i (m^3/s), $\bar{q}$ represents the average discharge of the observed hydrograph (m^3/s), and N is the number of data. The CE quantifies the goodness of fit between the estimated hydrograph and the observed hydrograph. A better fit is represented by a CE that is closer to unity.

Error of total volume, EV (%)

$$\mathrm{EV}(\%) = \frac{\sum_{i=1}^{N} [\hat{q}(i) - q(i)]}{\sum_{i=1}^{N} q(i)} \times 100\% \tag{11}$$

where $\hat{q}(i)$ denotes the discharge of the simulated hydrograph for time i (m^3/s), and $q(i)$ is the discharge of the observed hydrograph for time i (m^3/s). The EV specifies the mean error between the estimated hydrograph and the observed hydrograph. When the value of EV is positive, the mean estimated discharge exceeds the observed discharge, and vice versa. A better fit is represented by a smaller absolute value of EV.

The error of peak discharge, EQ_P (%)

$$\mathrm{EQ_P}(\%) = \frac{\hat{q}_\mathrm{P} - q_\mathrm{P}}{q_\mathrm{p}} \times 100\% \tag{12}$$

where $\hat{q}_\mathrm{P}$ denotes the peak discharge of the simulated hydrograph (m^3/s), and q_P is the peak discharge of the

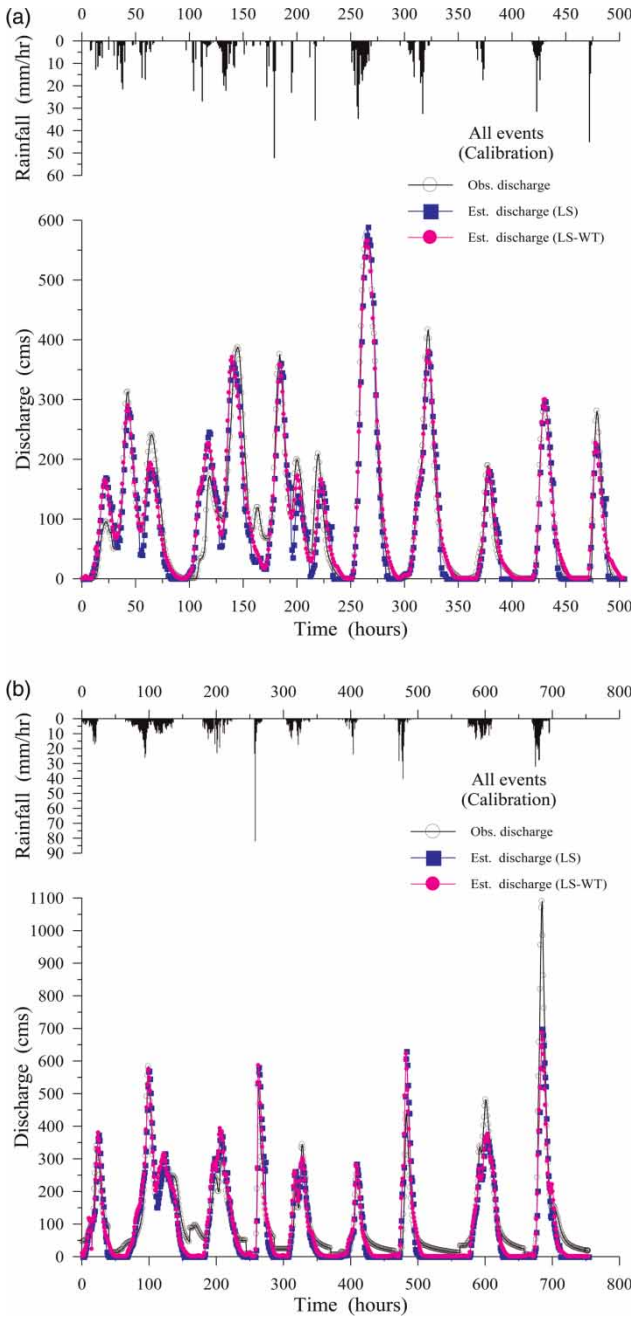

Figure 3 | Calibrated hydrographs for all events in series. (a) Feng-Hua Bridge Watershed. (b) Wu-Tu Watershed.

observed hydrograph (m^3/s). When EQ_P is positive, the estimated peak discharge exceeds the observed peak discharge. When EQ_P is negative, the estimated peak discharge is smaller than the observed peak discharge. A better fit is represented by a smaller absolute value of EQ_P.

The error of the time for peak to arrive, ET_P

$$ET_P = \hat{T}_P - T_P \tag{13}$$

where $\hat{T}_P$ denotes the time for the simulated hydrograph peak to arrive (hours), and T_P represents the

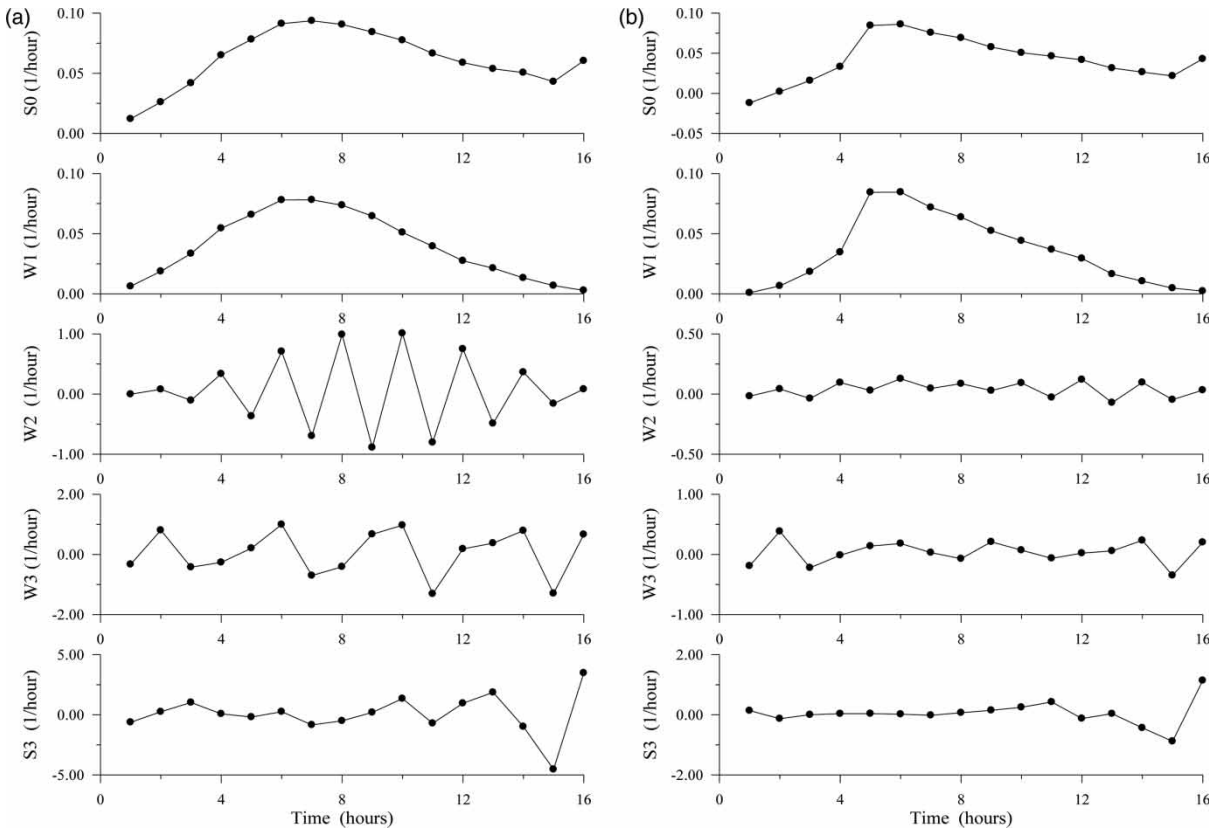

Figure 4 | The estimated system and subsystem response functions at various scales from the calibration data. (a) Feng-Hua Bridge watershed. (b) Wu-Tu watershed.

Table 4(a) | The validation results using LS and LS-WT for the Feng-Hua Bridge watershed

Event	EV (%) LS	LS-WT	CE LS	LS-WT	COR LS	LS-WT	EQ_P (%) LS	LS-WT	ET_P (h) LS	LS-WT
TIM	4.98	−0.36	0.829	0.889	0.918	0.946	2.51	1.00	0	−1
CAITLIN	4.96	−0.83	0.924	0.955	0.963	0.977	0.63	1.33	−2	−2
DOUG	4.95	−0.14	0.876	0.907	0.939	0.955	−12.13	−13.22	0	0
HERB	5.01	−0.30	0.937	0.971	0.971	0.988	−5.58	−13.13	−5	−3
STORM (1999/08/10)	4.93	−0.44	0.683	0.739	0.937	0.950	45.50	47.33	0	−1
STORM (2000/07/27)	5.22	−0.23	0.857	0.873	0.927	0.937	−3.56	−0.47	−2	−2
BILIS	4.92	−0.88	0.877	0.913	0.971	0.979	14.59	12.77	0	0
Average	4.996	0.454	0.855	0.892	0.947	0.962	12.071	12.750	1.286	1.286

Note: The columns for EV, EQ_P, and ET_P all contain negative values, and present the average of the absolute values.

Table 4(b) | The validation results using LS and LS-WT for the Wu-Tu watershed

Event	EV (%)		CE		COR		EQ_P (%)		ET_P (h)	
	LS	LS-WT	LS	LS-WT	LS	LS-WT	LS	LS-WT	LS	LS-WT
ZANE	19.07	14.45	0.882	0.906	0.958	0.964	−16.94	−17.21	0	0
WINNIE	−8.31	−14.40	0.891	0.891	0.945	0.948	−19.44	−20.10	1	1
STORM(1998/10/04)	20.97	16.51	0.869	0.879	0.968	0.962	−7.77	−4.17	1	1
ZEB	15.81	11.06	0.937	0.949	0.977	0.979	−0.33	−1.65	1	1
BABS	23.87	19.57	0.763	0.797	0.906	0.914	−24.31	−22.3	3	3
STORM(1999/12/13)	9.13	3.99	0.876	0.893	0.945	0.950	4.84	6.62	5	5
KAI-TAK	−17.33	−23.90	0.598	0.658	0.879	0.910	4.00	6.81	3	3
BEBINCA	22.70	18.36	0.696	0.705	0.881	0.872	−29.12	−28.4	4	4
STORM(2000/11/16)	20.55	15.91	0.458	0.590	0.913	0.936	19.93	17.99	2	2
Average	17.527	15.350	0.774	0.808	0.930	0.937	14.076	13.917	2.222	2.222

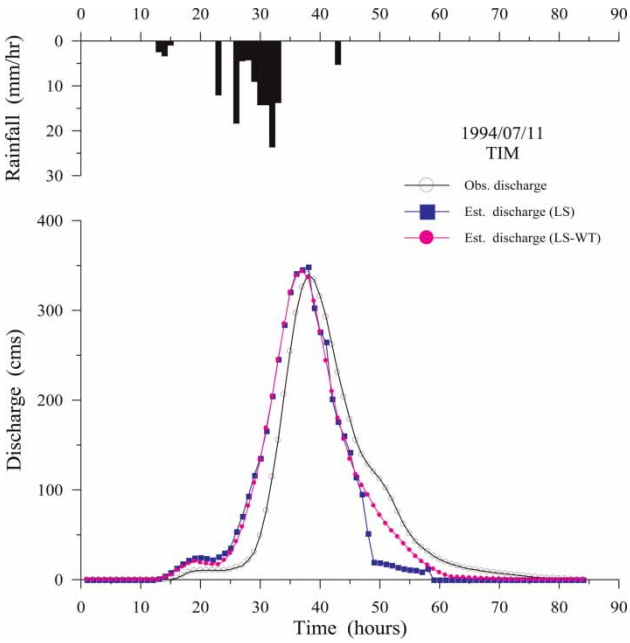

Figure 5 | Validated hydrographs of the Feng-Hua Bridge watershed for Typhoon TIM, 1994.

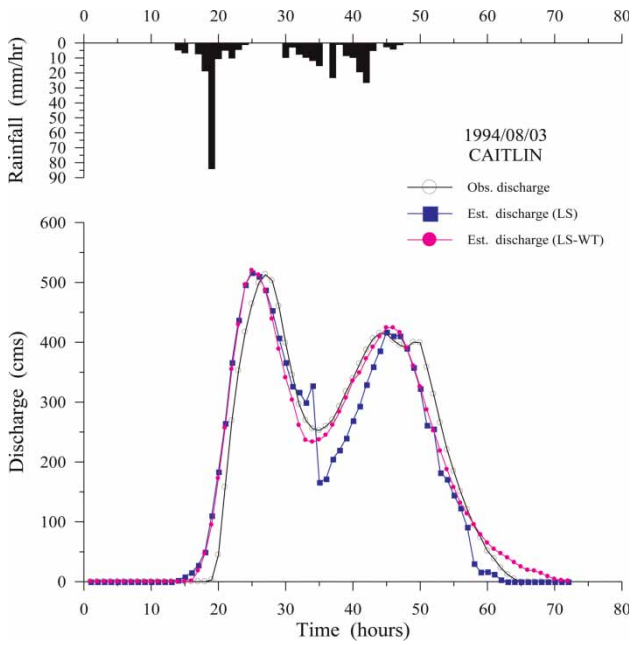

Figure 6 | Validated hydrographs of the Feng-Hua Bridge watershed for Typhoon CAITLIN, 1994.

time required for the observed hydrograph peak to arrive (hours). When ET_P is negative, the estimated peak discharge precedes the observed peak discharge. When ET_P is positive, the estimated peak discharge follows the observed peak discharge. A better fit is represented by a smaller absolute value of ET_P.

Correlation coefficient, COR

$$\mathrm{COR} = \frac{\sum_{i=1}^{N} [q(i) - \bar{q}][\hat{q}(i) - \bar{\hat{q}}]}{\sqrt{\sum_{i=1}^{N} [q(i) - \bar{q}]^2 \sum_{i=1}^{N} [\hat{q}(i) - \bar{\hat{q}}]^2}} \tag{14}$$

where $\hat{q}(i)$ denotes the discharge of the simulated hydrograph for time i (m^3/s), $q(i)$ is the discharge of the observed hydrograph for time i (m^3/s), $\bar{q}$ and $\bar{\hat{q}}$ represent the average discharge of the observed and simulated hydrograph (m^3/s), respectively, and N is the number of data. The COR quantifies the measure of the linear association between the estimated and observed hydrograph. A better fit is represented by a COR that is closer to unity.

RESULTS AND DISCUSSION

In this study, effective rainfall and direct runoff time series data were decomposed using *à trous* WT to obtain an approximate signal (S3) and detailed signals (W1–W3). In this study, the *à trous* WT with a wavelet function related to a B_3 spline function was selected because it is of compact support (necessary for a WT) and is point-symmetric. The number of scales was set to three according to previous studies (Chou 2011a, b). Calibrated typhoon events were connected in series as a single typhoon event to determine the representative average of the subsystem response function at each scale. Figure 2 shows the 3-level decomposition results for the calibration data on the Feng-Hua Bridge and Wu-Tu watershed. Notably, S0 denotes the original rainfall or runoff time series. The trend in calibrated rainfall data obtained by WT resembles that of calibrated runoff data at each scale. These analytical results confirm that WT is effective for simultaneously decomposing rainfall and runoff time series data. The decomposed rainfall and runoff time series can identify the subsystem response functions to enable obtainment of the characteristics at various scales.

Table 3 shows the calibration results of the LS and the LS-WT. Calibration results on Feng-Hua Bridge and Wu-Tu watershed show that EV, CE, and COR values are slightly better in the LS-WT than in the LS. For the EQ_P criterion, the value obtained by the LS-WT is slightly worse than that of the LS. Based on the ET_P criterion, the value obtained by the LS-WT is identical to that obtained by the LS. The calibration results, as plotted in Figure 3, show marginal improvement over traditional LS approaches. However, the runoff hydrograph estimated by the LS-WT is smoother than that obtained using the LS, especially in the recession limb.

The estimated system (S0) and subsystem (W1, W2, W3, and S3) response functions obtained from multiple typhoon events at various scales are plotted in Figure 4. Durations of the system and subsystem response functions are calculated as the difference between the durations of effective rainfall and direct runoff (Singh 1988). The estimated system and subsystem response functions can be used for performance comparisons of the LS and LS-WT. In addition to providing validation data for the proposed approach, the estimated system and subsystem response functions provide average characteristics of system and subsystems, respectively.

Table 4 shows the validation results when using the LS and LS-WT. The data on the Feng-Hua Bridge watershed show that the average absolute value of EV obtained by the LS-WT (0.454%) is better than that obtained by the LS (4.996%). For the CE criterion, the average value obtained by the LS-WT (0.892) is better than that obtained by the LS (0.855). For the COR criterion, the average value obtained by the LS-WT (0.962) is greater than that obtained by the LS (0.947). For each event, the LS-WT also outperforms the LS on EV, CE, and COR. For the EQ_P criterion, the average absolute value of the LS-WT (12.750%) is slightly worse than that of the LS (12.071%). For the ET_P criterion, the LS-WT (1.286 h) performs comparably to the LS (1.286 h).

The data on the Wu-Tu watershed show that the average absolute value of EV obtained using the LS-WT (15.350%) is slightly better than that obtained by the LS (17.527%). For the CE criterion, the average value obtained by the LS-WT (0.808) is better than that obtained by the LS (0.774). For the COR criterion, the average value obtained by the LS-WT (0.937) is slightly greater than that obtained by the LS (0.930). For the EQ_P criterion, the average absolute value of the LS-WT (13.917%) is slightly better than that of the LS (14.076%). For the ET_P criterion, the LS-WT (2.222 h) performs the same as the LS (2.222 h).

These results show that, because the LS-WT includes several components at various scales, it simulates the rainfall–runoff relationship slightly more accurately, compared with the LS, which includes only single time series at the original scale. These calibration and validation results also show the effectiveness of the proposed LS-WT in identifying the rainfall–runoff relationship.

Figures 5–7 and Figures 8–10 display three representative validation results in Feng-Hua Bridge and Wu-Tu watershed, respectively. Figure 5 shows that the runoff hydrograph estimated by the LS-WT is smoother than that obtained using LS, especially in the recession limb between time indices 38 and 58. Figure 6 shows a drop in the runoff hydrograph estimated by the LS between time indices 34 and 35. However, the runoff hydrograph estimated by the LS-WT is smooth and fits the observed data. Figure 7 shows that the results simulated using the LS produces easily shocked hydrographs, especially in the valley and recession limb, whereas the LS-WT yields smooth hydrographs. These findings show that in wavelet decomposition, the smoothing of detailed signals and the approximation improve with the number of scales. Furthermore, detailed signals, such as W1, W2, and W3, are dominated by noise and contribute little to the overall results. An approximation such as S3 represents the smooth trend of the overall results and yields a smoother hydrograph than when using the LS.

Figures 8 and 9 show that the estimated hydrograph obtained from the LS is slightly uneven. In contrast, the estimated hydrograph obtained from the LS-WT is smooth. Figure 10 shows that the runoff hydrographs obtained using the LS-WT fit the observed data more closely than those obtained using the LS between time indices 57 and 66. In addition, a drop exists in the runoff hydrograph estimated by the LS between time indices 77 and 79. However, the runoff hydrograph estimated by the LS-WT is smooth. As expected, wavelet decomposition smoothes

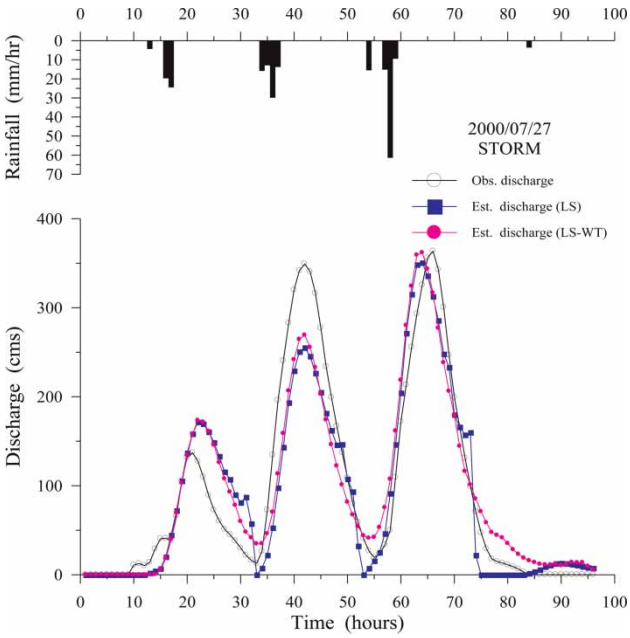

Figure 7 | Validated hydrographs of the Feng-Hua Bridge watershed for STORM (2000/07/27), 2000.

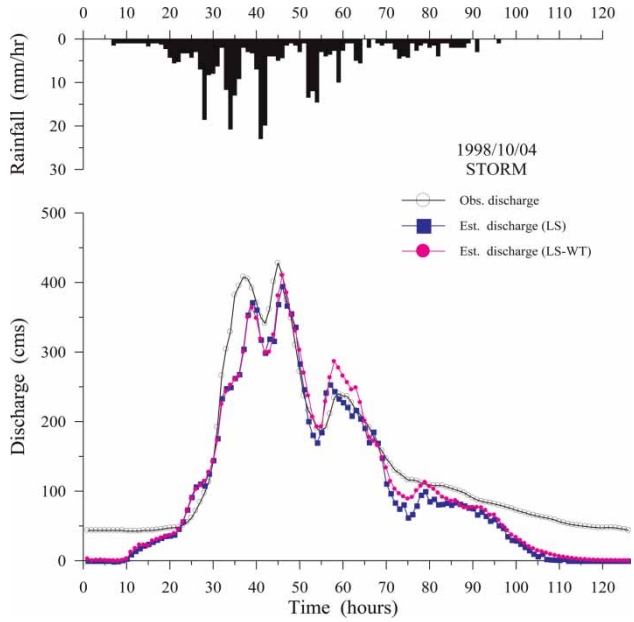

Figure 8 | Validated hydrographs of the Wu-Tu watershed for STORM (1998/10/04), 1998.

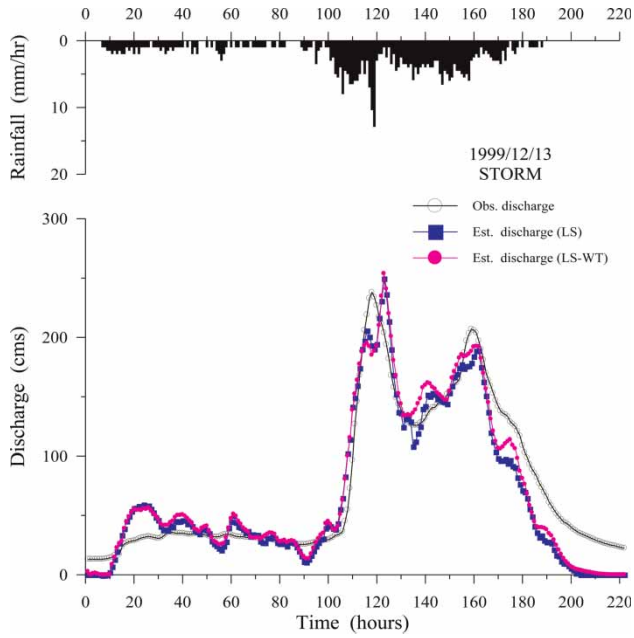

Figure 9 | Validated hydrographs of the Wu-Tu watershed for STORM (1999/12/13), 1999.

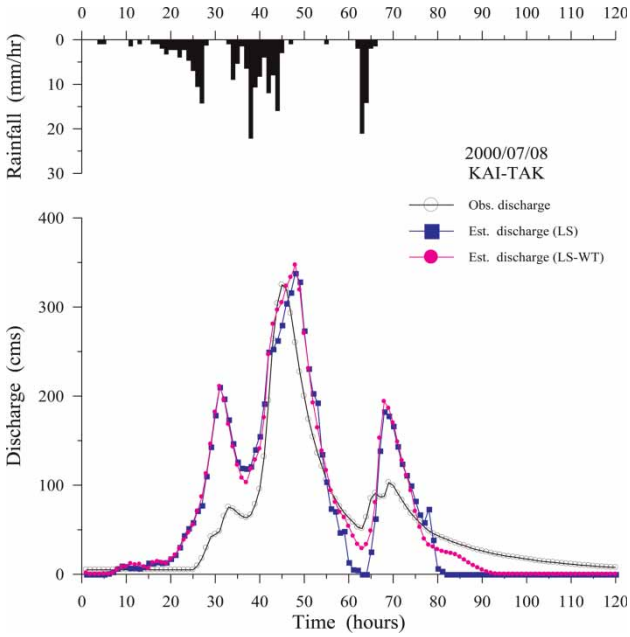

Figure 10 | Validated hydrographs of the Wu-Tu watershed for Typhoon KAI-TAK, 2000.

the hydrographs, which may help in building a more meaningful (robust) model.

Wavelet functions and WT have various forms. Selections of wavelet function and WT are critical and depend on the object of the transform, such as the information to be captured. The proposed approach uses the WT of the hydrological time series to analyze rainfall–runoff processes at each scale. Accordingly, the *à trous* algorithm of the WT was selected because it is redundant and able to provide the detail signal by wavelet coefficients. Therefore, it captures small 'features' of interpretational value in the data (Murtagh 1998).

CONCLUSIONS

This study developed a novel wavelet-based method for enhancing the accuracy in modeling the rainfall–runoff relationship. First, the *à trous* WT decomposed the original effective rainfall and direct runoff data simultaneously. The decomposed rainfall and runoff time series calibrated the subsystem characteristics at each scale. The validated decomposed rainfall time series were convoluted with the estimated subsystem response function to obtain estimated runoff at each scale. The estimated runoff at the original scale, which is compared with the observed runoff time series, can be obtained using wavelet reconstruction. The calibration and validation results for Feng-Hua Bridge and Wu-Tu watershed show that the proposed wavelet-based method slightly outperforms the traditional method using the data at the original scale. This is because of the MRA property of the WT.

Representative validation results for the Feng-Hua Bridge and Wu-Tu watershed also indicate that the results simulated using the LS may produce easily shocked hydrographs, whereas the LS-WT yields smooth hydrographs. This is because in wavelet decomposition, the smoothing of detailed signals and the approximation improve with the number of scales. Wavelet decomposition smoothes the hydrographs, which may build a more significant (robust) model.

This study applied WT for simultaneous decomposition of rainfall and runoff time series. The decomposed rainfall and runoff time series explore the subsystem characteristics at each scale. Validation results show that the average values of the calibrated subsystem response functions at each scale can represent the average system characteristics of each respective scale.

Numerous types of WT exist. In this study, the *à trous* WT is redundant and can provide the detail signal by wavelet coefficients. Therefore, it captures small features of interpretational value in the data, and is suitable for the modeling of the rainfall–runoff process at each scale. In addition, the proposed wavelet-based method using the multi-scale analysis differs substantially from conventional methods that use data at a single original scale.

REFERENCES

Aussem, A. & Murtagh, F. 2001 Web traffic demand forecasting using wavelet-based multiscale decomposition. *International Journal of Intelligent Systems* **16**, 215–236.

Chibani, Y. & Houacine, A. 2003 Redundant versus orthogonal wavelet decomposition for multisensor image fusion. *Pattern Recognition* **36**, 879–887.

Chou, C. M. 2007 Efficient nonlinear modeling of rainfall-runoff process using wavelet compression. *Journal of Hydrology* **332**, 442–455.

Chou, C. M. 2011a A threshold based wavelet denoising method for hydrological data modelling. *Water Resources Management* **25** (7), 1809–1830.

Chou, C. M. 2011b Wavelet-based multi-scale entropy analysis of complex rainfall time series. *Entropy* **13**, 241–253.

Holschneider, M. 1995 *Wavelets: An Analysis Tool*. Oxford University Press, New York.

Labat, D., Ababou, R. & Mangin, M. 2000 Rainfall-runoff relations for karstic springs. Part II: continuous wavelet and discrete orthogonal multiresolution analyses. *Journal of Hydrology* **238**, 149–178.

Lane, S. N. 2007 Assessment of rainfall-runoff models based upon wavelet analysis. *Hydrological Processes* **21** (5), 586–607.

Lee, X. B., Zheng, J. & Lee, H. Q. 1999 Combination forecasting using ANN based on wavelet transform series. *Journal of Hydraulical Engineering* **2**, 1–4 (In Chinese).

Mallat, S. G. 1989 A theory for multiresolution signal decomposition: the wavelet representation. *IEEE Transactions on Pattern Analysis and Machine Intelligence* **11** (7), 674–693.

Murtagh, F. 1998 Wedding the wavelet transform and multivariate data analysis. *Journal of Classification* **15**, 161–183.

Nakken, M. 1999 Wavelet analysis of rainfall–runoff variability isolating climatic from anthropogenic patterns. *Environmental Modelling and Software* **14**, 283–295.

Nourani, V., Komasi, M. & Mano, A. 2009 A multivariate ANN-wavelet approach for rainfall–runoff modeling. *Water Resources Management* **23** (14), 2877–2894.

Rao, R. M. & Bopardikar, A. S. 1998 *Wavelet Transforms, Introduction to Theory and Applications*. Addison-Wesley, USA.

Sherman, L. K. 1932 Streamflow from rainfall by the unit-graph method. *Engineering News Record* **108**, 501–505.

Singh, V. P. 1988 *Hydrology System, Vol. 1 Rainfall-Runoff Modeling*. Prentice Hall Inc. Publishing, New Jersey.

Wang, W. S., Ding, J. & Lee, Y. Q. 2005 *Hydrological Wavelet Analysis*. Chemical Industry Press, Beijing (In Chinese).

Wei, Y. X. & Wang, L. X. 2005 *Engineering Hydrology*. Water Conservancy and Electricity Press, Beijing (In Chinese).

Zhang, J. C., DeAngelis, D. L. & Zhuang, J. Y. 2011 *Theory and Practice of Soil Loss Control in Eastern China*. Springer, New York.

First received 26 February 2012; accepted in revised form 30 May 2012. Available online 9 October 2012